Available online at www.sciencedirect.com
ScienceDirect
Journal of Molecular Graphics and Modelling 26 (2007) 691–699
Journal of Molecular Graphics and Modelling
www.elsevier.com/locate/JMGM

Modelling the restoration of wild-type dynamic behaviour in ΔF508-CFTR NBD1 by 8-cyclopentyl-1,3-dipropylxanthine

Daniel J. Warner [a], Manish M. Vadolia [a], Charles A. Laughton [a], Ian D. Kerr [b], Stephen W. Doughty *

[a] *Centre for Biomolecular Sciences, School of Pharmacy, University of Nottingham, Nottingham NG7 2RD, UK*
[b] *School of Biomedical Sciences, University of Nottingham, Nottingham NG7 2RD, UK*

Accepted 19 April 2007
Available online 24 April 2007

Abstract

Cystic fibrosis (CF) is the most frequently occurring severe, genetic disease in western populations with an incidence as high as 1 in 2500. The principal biochemical defect in CF is a mutation in a membrane transport protein, namely the cystic fibrosis transmembrane conductance regulator (CFTR), which is responsible for the conductance of chloride ions across cell membranes. In 70% of cases a single mutation in CFTR, namely the deletion of amino acid 508 (called ΔF508) is sufficient to cause severe disease. This mutation manifests as a failure of the protein to be effectively targeted to the membrane. Recently, it has been shown that small molecule drug therapy can restore the membrane-targeting of ΔF508-CFTR, where the mutant channel functions adequately.

We have created models of the first nucleotide-binding domain (NBD1) region (which houses the proposed binding site of these restorative drugs) of the wild-type and mutant forms of human CFTR. We have simulated the dynamical behaviour of these proteins in the presence of drugs that restore trafficking of the protein. Our results indicate that there are particular modes of dynamic motion that are distinguishable between wild-type and mutant CFTR. These regions of motion are localized in the regions of the ΔF508 mutation and the drug-binding regions. The simulations of drug binding indicate that wild-type dynamic motions are restored in these regions. We conclude therefore that these drugs are able to alter the dynamic properties of ΔF508-CFTR such that the drug-bound mutant protein more closely resembles the wild-type protein dynamic behaviour, and hence we hypothesize that it is this that allows for correct targeting to the membrane.

Keywords: Molecular dynamics; Cystic fibrosis; Essential dynamics; NBD1; CPX

1. Introduction

Cystic fibrosis (CF) is the commonest fatal, autosomal recessive disease affecting people of north European descent. Mutations in the gene coding for the cystic fibrosis transmembrane conductance regulator (CFTR) manifest as chronic lung infections and loss of pancreatic function, both resulting from abrogated epithelial plasma membrane chloride ion transport [1,2], and a consequent loss of integrity of epithelial secretions. CFTR is a member of the ATP-binding cassette (ABC) family of transporters, other members of which mediate diverse processes in prokaryotes and eukaryotes including nutrient uptake, insulin secretion and antigen processing [3]. A complete understanding of CFTR at a physiological, structural and dynamic level is necessary if the goal of directed pharmaceutical intervention of CF is to be realized. CFTR is a 1408 amino acid protein, which by sequence analysis is predicted to contain two membrane-spanning domains (MSDs), each followed by a cytoplasmic, nucleotide-binding domain (called NBD1 and NBD2) together with a regulatory ('R') domain situated between NBD1 and

Abbreviations: ΔF508, deletion Phe-508; ABC, ATP-binding cassette; CF, cystic fibrosis; CFTR, cystic fibrosis transmembrane conductance regulator; CPX, 8-cyclopentyl-1,3-dipropylxanthine; MD, molecular dynamics; MSD1/MSD2, membrane-spanning domains 1&2; NBD1/NBD2, nucleotide-binding domains 1&2; PCA, principal component analysis; RMSD, root mean square deviation; RMSIP, root mean square inner product

* Corresponding author. Current address: Faculty of Health and Biological Sciences, School of Pharmacy, University of Nottingham Malaysia Campus, Jalan Broga, 43500 Semenyih, Selangor Darul Ehsan, Malaysia.
Tel.: +60 3 8924 8200; fax: +60 3 8924 8018.
E-mail addresses: stephen.doughty@nottingham.ac.uk, stephen.doughty@nottingham.edu.my (S.W. Doughty).

1093-3263/$ – see front matter © 2007 Elsevier Inc. All rights reserved.
doi:10.1016/j.jmgm.2007.04.005

MSD2. At the structural level CFTR has recently been imaged by low resolution electron microscopy which suggests that its overall architecture is shared with other ABC transporters for which similar data exists [4]. No high resolution data for the entire protein is available. Conversely, recent atomic resolution data has been obtained for the N-terminal NBD (NBD1) of murine CFTR [5].

The commonest disease-causing mutation, *del*1653–1655, occurring in about 70% of CF cases, occurs within NBD1 and results in deletion of Phe-508, ΔF508. It has been shown that this mutant isoform is defective both in terms of trafficking to the plasma membrane and in terms of its channel kinetics [6–9]. Failed trafficking resulting in the formation of aggregated proteins (aggresomes) [10,11], can be partially restored *in vitro* through a reduction in temperature [12], and more recently it appears that small molecule drug therapy (e.g. benzo(c)quinoliziniums) such as MPB-07 and xanthines such as 8-cyclopentyl-1,3-dipropylxanthine (CPX, Fig. 1), can lead to plasma membrane localization [13,14]. Pertinently, it has been shown that CPX binds to NBD1 of CFTR and that there is differential binding to ΔF508 NBD1 [15]. Moreover, studies of isolated NBD1 of CFTR have demonstrated that the thermodynamic stability of wild-type and ΔF508 forms of NBD1 are similar, but that the folding pathway of the mutated NBD1 was different from the wild-type NBD1 [16,17]. This is consistent with a hypothesis in which intra-domain dynamics differ between wild-type and mutant NBD1. The latter may lead to altered inter-domain dynamics, with subsequent recognition of CFTR by enzymes of the ubiquitin proteasome system [11]. The correction of NBD1 intra-domain dynamics by small molecule therapy, such that the dynamic behaviour of ΔF508 CFTR more closely resembling the dynamic behaviour of the wild-type protein, may circumvent this recognition.

Previous attempts to elucidate structural differences between wild-type and mutant CFTR have focused upon the production of static models [18,19], which though providing some valuable insights were hampered by the fact that residue 508 actually lies in a rather poorly conserved region of the ABC transporter NBD fold [20]. In the current manuscript, we have taken an alternative approach, viz, to investigate the differences between the dynamic fluctuations of wild-type and mutant CFTR NBD1, and the effect of drug binding on these dynamic fluctuations. We have constructed molecular models of human CFTR NBD1 and the ΔF508 mutant isoform (based upon the murine NBD1 crystal structure [5]) and performed molecular dynamics simulations with subsequent characterization of the dynamic behaviour by principal component analysis. This analysis indicates that wild-type and mutant ΔF508 NBD1 can be distinguished by altered dynamics, in parallel with their *in vitro* distinct folding kinetics. Moreover, the presence of the small molecule CPX docked into the mutant NBD1 protein produced an alteration of the dynamic behaviour of this domain, such that it now resembled the dynamic behaviour of the wild-type domain. The importance of this data in terms of understanding small molecule treatment of protein dysfunctional dynamics is discussed.

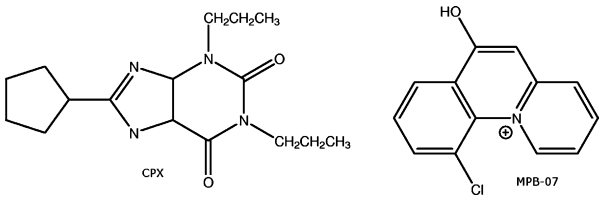

Fig. 1. Structures of CPX and MPB-07.

2. Methodology

2.1. Model building and docking of CPX

The structure of NBD1 from human CFTR was modelled using the available crystal structure of mouse CFTR NBD1 (PDB code 1R10; chain A at 3.0 Å resolution) [5]. The corresponding protein sequences were obtained from the SWISSPROT database and aligned (see Fig. 2). The sequence alignment showed that the mouse structure is a valid template to use, given that the alignments have sequence identity and similarity values of 79% and 93% respectively and no insertions or deletions. The use of a CFTR NBD1 structural template is a significant improvement over previous CFTR modelling exercises using other ABC-family structures (e.g. bacterial HisP) for homology modelling. The program Sybyl [21] was used to mutate the side-chains of the mouse structure such that they corresponded to the human CFTR NBD1 sequence. The mouse structure lacks a loop region between positions Q413 and V428, hence the 'loop search' facility was employed to construct this loop within the human model. The original crystal structure of the mouse NBD1 contained an ATP molecule, so this was deleted to give the apo-wild-type starting structure. Prior to minimization and geometry optimization an initial chirality and structural integrity check was performed in order to ensure the validity of the starting model.

This starting structure was further mutated in order to produce a ΔF508 CFTR NBD1 structure. This model was constructed by deleting residues 503 through to 510 and then replacing that region without the F508 residue, using the Sybyl loop-search facility. Two models were generated; one of the apo-ΔF508 CFTR NBD1 and another where CPX was docked in to the ATP-binding site of the model. This docking was performed by manual superimposition of the heterocyclic rings of CPX and the ATP from the original structure.

Hence three models were generated prior to geometry optimization; namely apo-wild-type NBD1, apo-ΔF508 CFTR NBD1 and CPX-bound ΔF508 CFTR NBD1. Each model was then subjected to an initial minimization within Sybyl using the Tripos forcefield to resolve any initial clashes (100 iterations of Powell minimization). This was followed by parameterization of the CPX molecule for further minimization and molecular dynamics simulations.

Following completion of the work presented here, crystal structures for human CFTR ΔF508 and F508A NBD1 domains were reported and made available [22] (PDB codes 1XMI and 1XMJ). Our refined models prove very consistent with these structures (see Table 1). The RMSDs typically lie within the range of RMS fluctuations observed in our MD trajectories, therefore we do not believe that the structural

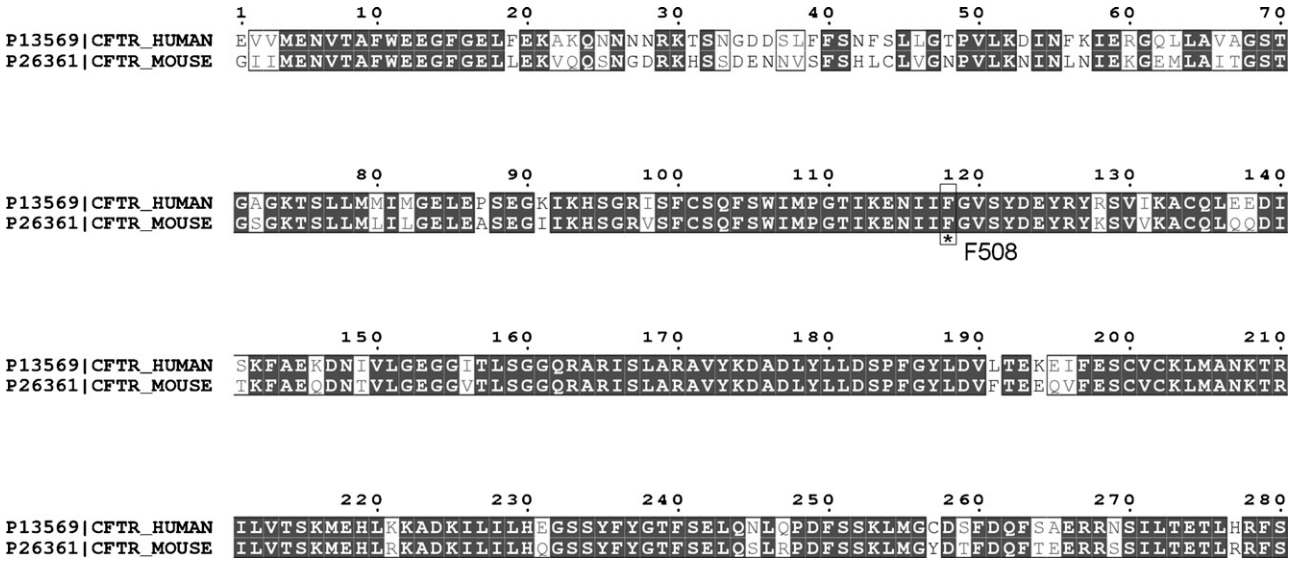

Fig. 2. Sequence alignment of NBD1 from mouse (CFTR_MOUSE; swissprot accession number P26361) and human (CFTR_HUMAN; swissprot accession number P13569) CFTR.

differences will significantly alter the dynamical behaviour we have observed.

2.2. Preparation of the systems for molecular dynamics

The coordinates for the CPX molecule were extracted from the PDB file containing the docked structure. Charges were calculated to fit the electrostatic potential at points selected according to the Merz–Singh–Kollman scheme [23,24] at the 6-31G* level *in-vacuo*. This calculation was performed using Gaussian 98 [25].

Parameterization of CPX was completed using the general Amber force field [26] within the antechamber module of AMBER 7 [27], with partial charges for each of the atoms generated using RESP [28]. In all three systems the protein was parameterized using the Amber 1994 force field [29], and solvated in a truncated octahedral water box containing ~6000 pre-equilibrated TIP3P water molecules [30]. Default ionization states were used for all residues. The structures were allowed to relax via 50 steps of steepest descents, followed by conjugate gradient minimization until the energy gradient had been reduced to 0.05 kcal mol^{-1}.

2.3. Molecular dynamics protocol

All simulations were performed at constant temperature and pressure, with a 2 fs timestep, and SHAKE to constrain all bonds to hydrogen at equilibrium values [31]. Electrostatics beyond an 8 Å cutoff were calculated by particle mesh Ewald [32], with the temperature coupled to an external bath using a weak coupling algorithm [33]. A 10 ps simulation was performed on the solvent at 100 K to stabilize interactions with the protein. The water was heated to 300 K over a further 20 ps, with a harmonic restraint of 100 kcal mol^{-1} $Å^{-2}$ to keep the protein (and in one case drug molecule) close to the original structure. These restraints were then gradually reduced over a further 30 ps, before allowing the simulation to run unrestrained for a period of 2.1 ns, during which coordinates were recorded every 1 ps. The first 100 ps of each unrestrained trajectory was discarded to allow for equilibration, leaving a

Table 1
RMSD comparisons (Cα atoms only) between modelled structures with structures taken from the Protein Data Bank

Model	Mouse		Human F508A[a]					Human ΔF508
	$1R10_A$	$1R10_B$	$1XMI_A$	$1XMI_B$	$1XMI_C$	$1XMI_D$	$1XMI_E$	$1XMJ_A$
Minimised								
Wild-type protein	0.44	0.49	1.02	1.13	0.99	1.01	1.03	1.59
ΔF508 mutant (CPX absent)	1.03	1.06	1.49	1.58	1.45	1.48	1.49	1.84
ΔF508 mutant (CPX present)	1.02	1.05	1.47	1.57	1.45	1.47	1.47	1.83
Average								
Wild-type protein	1.91	1.95	1.46	1.51	1.47	1.44	1.48	1.84
ΔF508 mutant (CPX absent)	1.79	1.83	1.94	2.04	1.93	1.93	1.97	2.12
ΔF508 mutant (CPX present)	2.13	2.19	2.26	2.33	2.29	2.25	2.33	2.64

Only residues present in all structures within a given PDB entry were considered.

[a] Residues 401–435 and 640–670 inclusive were discarded for comparisons with 1XMI. This was due to the alternative orientation of these parts of the protein compared to both our model and the other two PBD entries.

2 ns 'production run' for each system on which the analysis presented here is based.

2.4. Analysis

Trajectory analysis was performed within the ptraj module of AMBER 8 [34]. To facilitate comparison between the systems all water molecules were removed from the trajectories, along with residue 118 (Phe-508) from the wild-type simulation and CPX molecule from the drug-bound simulation. Average structures were then calculated for each system both individually and for the three simulations combined. RMSD of Cα atoms and per-residue RMSF calculations were both performed using ptraj.

$$\mathrm{RMSD} = \left(\frac{1}{N} \sum_{i}^{n} (r_i - \langle r \rangle)^2 \right)^{1/2} \quad (1)$$

where r_i gives the coordinate for a given atom and $\langle r \rangle$ the average coordinate.

In assessing the stability of the simulations, the RMSD was calculated as in Eq. (1) with each frame being compared to the average structure from the three simulations combined. Only backbone Cα atoms were considered in this analysis.

Principal component analysis (PCA) was also performed using ptraj, based on the coordinates of the backbone N, C, Cα and O atoms, with all three trajectories fitted to the combined reference structure. Two rounds of PCA were completed with the objective of first investigating the difference between the structures generated during the course of the simulations, and the second to analyse the dynamic behaviour of each of the three individual systems. The first of these investigations involved concatenation of all three series of coordinates into a single trajectory. Calculation of the covariance matrix was then based on this extended trajectory, such that the eigenvectors describe the principal differences between the three simulations, as opposed to their dynamic modes. The second round of PCA was performed on each individual simulation, so as to elucidate the low frequency oscillations within a given system. The similarity between the sets of eigenvectors generated by this method was compared by calculating the inner product matrices, and also the RMSIP for the eight most significant vectors (Eq. (2)).

$$\mathrm{RMSIP} = \left(\frac{1}{8} \sum_{i=1}^{8} \sum_{j=1}^{8} (\eta_i \cdot \nu_j)^2 \right)^{1/2} \quad (2)$$

where η_i and ν_j represent the ith and jth eigenvectors respectively from the two simulations being compared.

2.5. Visualization and figure generation

Molecular graphics images were produced using the UCSF Chimera [35] package from the Computer Graphics Laboratory, University of California, San Francisco (supported by NIH P41 RR-01081). Graphs were produced using gnuplot version 3.7.

3. Results and discussion

3.1. Rationale behind use of molecular dynamics approach

NBDs of ABC transporters are currently believed to undergo a change in association in the presence of nucleotide substrate [36]. In most models, an inter-digitated NBD dimer is formed in the presence of ATP and sandwiches two molecules of ATP at the NBD:NBD interface [36]. In the current simulations, we have represented the monomeric NBD1 with no ATP bound. We believe that this represents the most appropriate starting point for these simulation studies for two main reasons. Firstly, we are not seeking to investigate dynamic changes occurring as a result of nucleotide binding and hydrolysis. Indeed, analysis of isolated NBD1 (wild-type and ΔF508) suggests that ATP binding is not compromised by the mutation [37,38]. Neither are we attempting to propose domain:domain interactions that may be altered as a result of CPX binding to NBD1, since the lack of high resolution structural detail on domain:domain interactions in CFTR precludes such an analysis [4]. Rather, we have investigated the intra-domain dynamic behaviour of CFTR-NBD1 in three separate simulations, in order to probe the effect of mutation from wild-type protein to ΔF508 mutant, and secondly the effect of binding CPX to the mutant protein. The first system contained a model of the wild-type protein (280 residues, no drug), the second system the ΔF508 mutant (279 residues, no drug) and finally the CPX system which contained the ΔF508 mutant protein with the docked CPX drug molecule (279 residues, drug bound).

3.2. Structural stability and residue fluctuations

Fig. 3 shows the time dependence of the root mean square displacement (RMSD) of all the Cα atoms from the respective minimized starting structure. All three simulations have a backbone RMSD fluctuating in the region of ∼2.5 Å, showing them all to have similar displacements throughout the duration of these parts of the simulations.

The relative mobility of individual residues may be quantified through calculation of the RMSF for each residue in turn (Fig. 4). The simulation of the mutant protein shows a particularly high degree of flexibility for residues in the region of the CPX binding site (residues 400–430), and also in the loop region surrounding the site of the mutation (residue 508). The high degree of movement in residues 400–430 is perhaps slightly unexpected, not least because these residues exhibit a significant degree of secondary structure, forming the α-helices which sandwich the drug against the bulk of CFTR-NBD1. A closer look at the structure reveals how in the absence of a molecule in the binding groove, the two helices are somewhat separated from the remainder of the protein, essentially forming an extended loop, providing some justification for this behaviour. It is highly likely that the high degree of mobility of this loop explains its omission in the crystallographic studies of this domain.

It is apparent from Fig. 4 that those regions of the protein highlighted above as being particularly flexible in the ΔF508

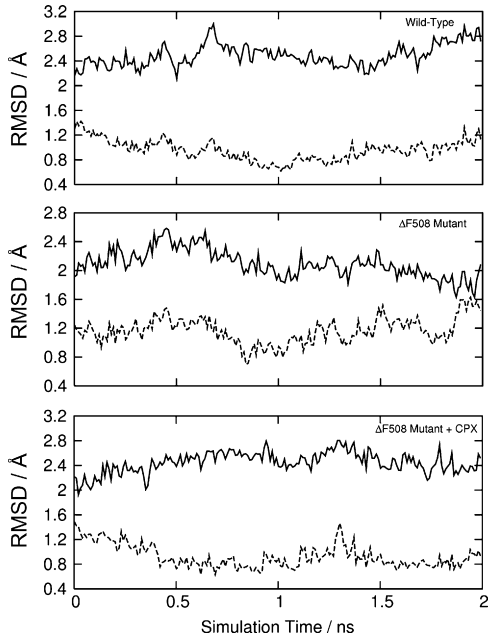

Fig. 3. RMSD of Cα atoms in comparison to the minimised starting structure (solid line) and the average structure (dotted line). Plots are shown for: the wild-type protein; ΔF508 mutant without the drug; ΔF508 mutant protein with the CPX drug bound.

mutant simulation, are considerably less mobile in the other two systems studied. This is interesting as it provides us with a potential mechanism by which binding of CPX to the mutant protein alters its dynamic behaviour such that the complex now more closely resembles the wild-type protein, as opposed to the mutant system in which the drug was absent. It is simple to see how a small molecule in the binding groove could have the

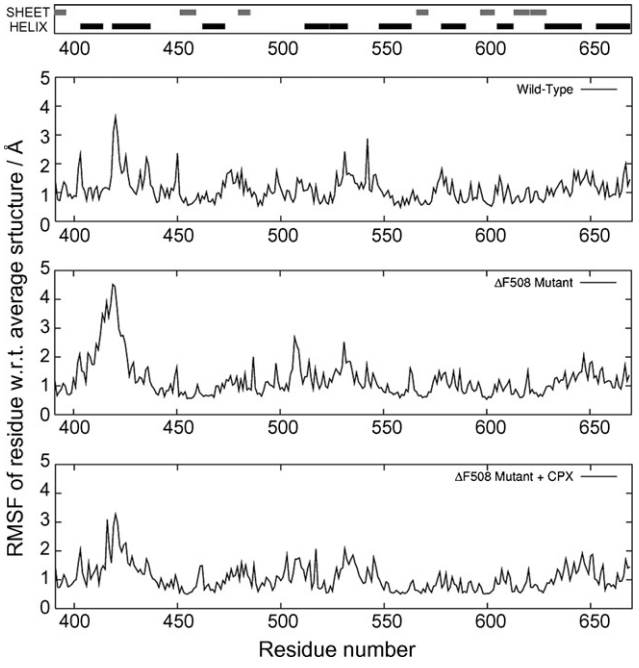

Fig. 4. Per-residue RMSF of all protein atoms from the average structure for that simulation. Plots are shown for: the wild-type protein; ΔF508 mutant without the drug; ΔF508 mutant protein with the CPX drug bound.

effect of suppressing the mobility of residues within its immediate vicinity, although what is perhaps more interesting is the process by which the presence of Phe-508 in the wild-type system is able to invoke the similar effect.

3.3. Principal component analysis

Principal component analysis (PCA) provides a powerful means of analyzing molecular dynamics simulations of biomolecules [39–41]. The process involves diagonalisation of the Cartesian covariance matrix, thus generating a series of eigenvectors such that those vectors with the largest eigenvalues describe the most significant dynamic modes of the molecule. Comparison of the vectors generated from one simulation with another may then be made, allowing quantitative assessment of the similarity between the dynamics in two different systems [42,43].

3.4. Structural comparisons

Applying PCA to the trajectory containing data from all three simulations produces a series of vectors highlighting the structural differences between the three systems. A plot of the projections of each simulation onto these vectors results in a map of conformational space in which these differences may be clearly identified (Fig. 5a). This figure reveals three distinct regions of conformational space inhabited by the three forms of the protein. To the left of the plot lie the structures of the CPX-ΔF508 complex in blue, while the other two systems in red and green, both containing apo forms of the protein, lie to the right, suggesting that a subtle change in the structure occurs following ligand removal. Animation of the vector describing this change confirms the point (Fig. 5b), by illustrating how the binding groove adopts a closed conformation in the simulations of the two apo proteins, whilst adopting a more open conformation for the CPX bound mutant complex.

Distribution of the trajectory projections in relation to the second highest ranking component exploits an altogether different means of classifying the structures. The two simulations located in the top half of the plot represent the wild-type and drug-bound complex systems, leaving the apo mutant isolated at the bottom. Thus, the structural characteristics highlighted by this component reveal a way in which the deformed structure of the ΔF508 mutant protein is potentially ‘rescued’ by the drug, and subsequently restored to a conformation that more closely resembles the wild-type protein. Furthermore, visualisation of this component (Fig. 5c) shows the loop region surrounding the Phe-508 deletion (top-right) to be that which is most dramatically affected by the distortions along this vector. As a result, the distance between this loop and the turn between the two α-helices which encompass the ligand is significantly increased. This structural change implies that the loss of an interaction, due to mutation, between Phe-508 and this surrounding loop region of the protein is in some way compensated by the binding of CPX.

One of the most interesting aspects to this behaviour is the process by which a message is relayed from the drug-binding site to the region of the mutation, two reasonably distant parts

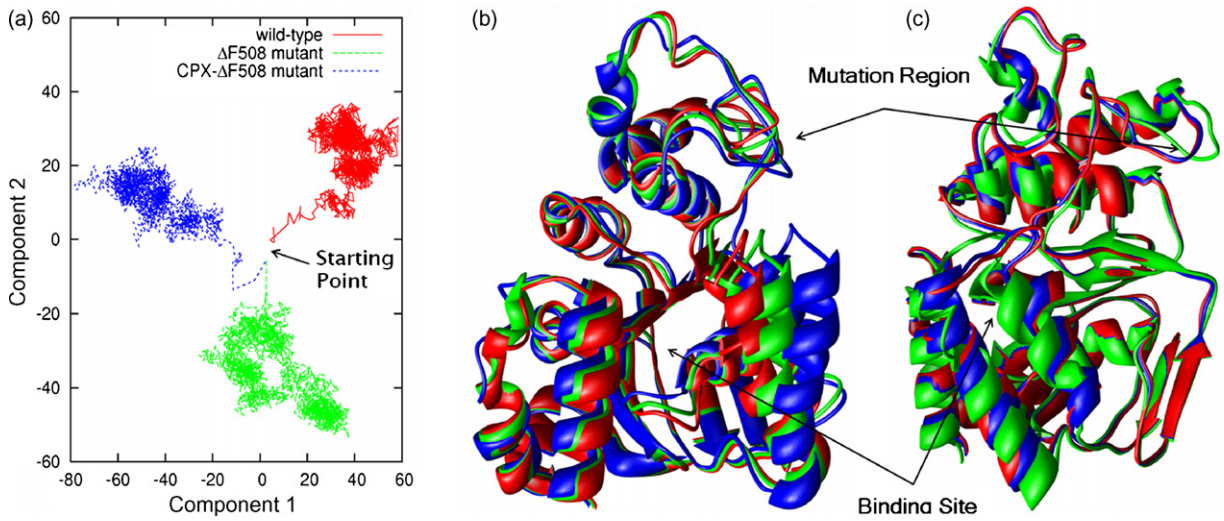

Fig. 5. Projection of structures onto the first two principal components of the backbone heavy atoms, as determined from the molecular dynamics simulations of CFTR NBD1. (a) Projections of the average structure from apo-wild-type (red), apo-ΔF508 mutant (green) and the CPX-ΔF508 complex (blue) simulations are shown with respect to the (b) first and (c) second component. The animations in (b) and (c) were derived from distortion of the average structure for all three simulations along the two highest ranking eigenvectors. The extent and direction of the distortion is determined by projection of the time-averaged structure for a given simulation onto these components.

of the molecule. Inspection of the structures at the atomistic level reveals how in the wild-type protein the Phe-508-containing loop appears to be stabilised through an interaction between the side-chains of Phe-508 and Trp-496. Furthermore, a requirement for this interaction for the correct folding of NBD1 was recently revealed in a series of NMR experiments by Thibodeau et al. [44].

In the simulation of the *apo*-mutant protein, the Trp-496 appears to compensate for the loss of Phe-508 through association with another neighbouring phenylalanine residue, Phe-494. This leaves the residues which make up the mutated loop free to move away from those parts of the protein which constitute the binding site. We have already seen from the backbone analysis how the introduction of CPX causes an opening of the ATP-binding site. A consequence of this is that Phe-494 adopts a new conformation, in which the side-chain atoms move inside the cleft. This transition once again leaves Trp-496 without a binding partner, and as a result, interactions between Trp-496 and the loop that encompasses the mutation are reformed. We hypothesise that the conformational change induced by the binding of CPX is transmitted to the region of the mutation via the side-chains of two interstitial residues, namely Phe-494 and Trp-496.

3.5. Dynamic comparisons

To further test the hypothesis that binding of CPX to the ΔF508 mutant has an effect on the dynamic behaviour of this protein, it was first necessary to perform PCA on each of the simulations individually. The backbone heavy atoms were all fitted to a common reference structure and the eight most significant modes from each simulation were calculated. Initial comparisons were first made through the calculation of the RMSIPs between the three simulations (Table 2), comparing the overall similarity between the eight highest ranking eigenvectors from each set, where a value of 1 indicates identical vector sets, while a value of 0 indicates the absence of any overlap what so ever. Intuitively, one might expect the two simulations of the empty protein to display the highest degree of subspace overlap, although this proves not to be the case. In fact, the RMSIP for all three simulation combinations is roughly the same. Although it is unlikely that there is any real significance in ranking the values presented in Table 2, it is still surprising to see such high similarity between the CPX-ΔF508 complex dynamics and those of the wild-type protein.

To probe further the origins of this similarity, and to identify the individual dynamic modes which were contributing to it, it was necessary to calculate the inner product of each individual pair of vectors. The result of this analysis (a matrix of inner products) is displayed in Fig. 6 in a graphical format. The most significant similarity observed between the wild-type dynamics and those of the empty mutant is found when comparing mode 2 from the wild-type simulation with mode 5 from that of ΔF508. These two modes show a high degree of similarity, with the red square indicating an inner product in the region of 0.53. Binding of CPX to the mutant induces interesting changes on the dynamics of the protein backbone. Although wild-type mode 2 appears to be conserved, in that there remains a high level of overlap between this vector and one calculated from the dynamics of the mutant, the promotion from 5th to 4th in the rankings suggests that this mode becomes marginally more

Table 2
RMSIP comparisons for the top eight ranking eigenvectors from simulations of CFTR NBD1

	Wild-type protein	ΔF508 mutant (CPX absent)
Wild-type protein	–	0.569
ΔF508 mutant (CPX present)	0.582	0.579

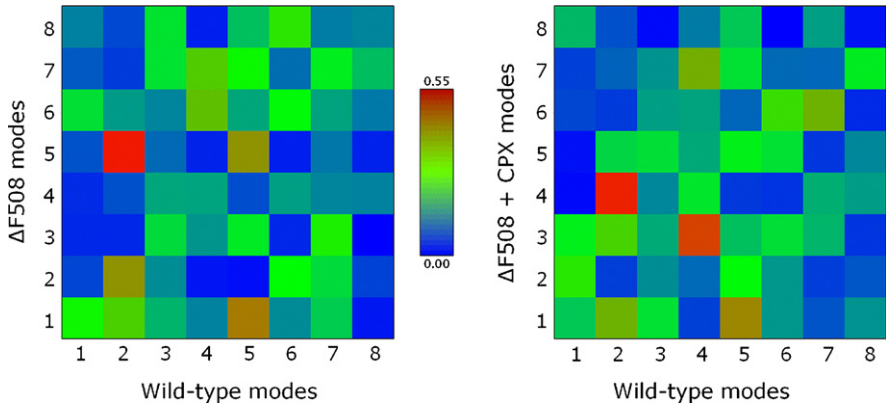

Fig. 6. Inner product matrices comparing the dynamic modes of wild-type protein with (left) ΔF508 mutant in the absence of the drug, and (right) ΔF508 mutant in the presence of the drug. Wild-type dynamic modes are displayed on the x-axis and mutant modes on the y-axis. Similarity of the vectors is graded by colour: blue indicates the least amount of similarity; followed by green; while the most similar vector pairs are coloured red.

significant. More interestingly, there now appears to be a high degree of similarity between wild-type mode 4 and mutant mode 3, a mode which was largely absent from the apo-mutant simulation. The reinstatement of this motion indicates a means by which binding of CPX restores wild-type protein-like dynamic behaviour to the simulation of the ΔF508 mutant.

Further investigation into the specific details of wild-type mode 4 reveals the identity of 30 residues which contribute most significantly to this particular motion (401, 413–418, 420–429, 431–438, 499, 510, 511, 542 and 669). Notably, those residues most prevalent in this motion are those within close proximity to the CPX binding site, and also, to a lesser extent, the region of the phenylalanine deletion. We propose therefore, that it is the restoration of this dynamic mode that accounts for the enhanced similarity between the CPX bound ΔF508-mutant and the wild-type protein dynamic behaviour, thus restoring 'wild-type' characteristic to the mutant protein.

4. Conclusion

Homology modelling based on the crystal structure of the mouse NBD1 proved successful in generating a model of the human form of the protein, with a structure that was stable throughout the course of a 2 ns MD simulation.

Analysis of the MD trajectories using PCA provided a description of the conformational space occupied by the three systems studied. The opening and closing of the ATP/CPX binding groove proved to be the most significant difference between the structures, allowing the two apo structures to be grouped together in one region of space, whilst the CPX-ΔF508 NBD1 complex exhibited the alternative open conformation. Although this distinction would not have been unexpected, the isolation of apo-ΔF508 NBD1 in a unique region of conformational space by the second ranked eigenvector probably would have been. This conformational motif not only relates both the apo-wild-type and drug-bound mutant structures at the exclusion of the apo mutant, but is actually localised in the region of the protein that is affected by the mutation. The postulation therefore, is that the presence of CPX brings about the restoration of wild-type structure to the mutated region of ΔF508 CFTR.

The PCA technique was used to examine the dynamic behaviour of each of the simulations in turn, and to quantitatively compare the principal modes of motion exhibited by the protein backbone's heavy atoms. Overall, the distinction between the RMSIPs for the three systems was only slight, although the similarity between the dynamic behaviour of the wild-type and CPX-ΔF508 NBD1 was greater than for any other combination. A heavy contribution to this similarity resulted from the restoration of one particular wild-type mode that was not prevalent in the apo-mutant simulation, but clearly observable in the drug-mutant complex.

In summary, there is considerable evidence from the MD simulations performed here that the association of CPX and ΔF508 NBD1 brings about significant changes to both the structure and dynamic behaviour of the mutated ΔF508 CFTR NBD1 domain. Moreover, the changes that occur in both the residue mobilities, and also the correlated motions of the main-chain heavy atoms, have been shown to make the drug-bound mutant domain behave more like the wild-type protein than the apo mutant does alone. It cannot be said from these simulations to what extent the observed dynamic behaviour is a product of the adoption of different conformations in each of the three systems, but it is proposed that a combination of these effects is responsible for the recognition of the drug-bound mutant domain as being 'like wild-type' as distinct from the lethal apo-mutant form.

Acknowledgements

DJW was supported through EPSRC studentship number RS2601/1. The authors would like to thank Dr. Ian Withers for use of the program 'viewgrid' to visualize the inner product matrices as shown in Fig. 6.

References

[1] B.S. Kerem, J.M. Rommens, J.A. Buchanan, D. Markiewicz, T.K. Cox, A. Chakravarti, M. Buchwald, L.C. Tsui, Identification of the cystic-fibrosis gene—genetic-analysis, Science 245 (1989) 1073–1080.

[2] J.R. Riordan, J.M. Rommens, B.S. Kerem, N. Alon, R. Rozmahel, Z. Grzelczak, J. Zielenski, S. Lok, N. Plavsic, J.L. Chou, M.L. Drumm, M.C. Iannuzzi, F.S. Collins, L.C. Tsui, Identification of the cystic-fibrosis gene-cloning and characterization of complementary-dna, Science 245 (1989) 1066–1072.
[3] C.F. Higgins, Abc transporters—from microorganisms to man, Annu. Rev. Cell Biol. 8 (1992) 67–113.
[4] M.F. Rosenberg, A.B. Kamis, L.A. Aleksandrov, R.C. Ford, J.R. Riordan, Purification and crystallization of the cystic fibrosis transmembrane conductance regulator (cftr), J. Biol. Chem. 279 (2004) 39051–39057.
[5] H.A. Lewis, S.G. Buchanan, S.K. Burley, K. Conners, M. Dickey, M. Dorwart, R. Fowler, X. Gao, W.B. Guggino, W.A. Hendrickson, J.F. Hunt, M.C. Kearins, D. Lorimer, P.C. Maloney, K.W. Post, K.R. Rajashankar, M.E. Rutter, J.M. Sauder, S. Shriver, P.H. Thibodeau, P.J. Thomas, M. Zhang, X. Zhao, S. Emtage, Structure of nucleotide-binding domain 1 of the cystic fibrosis transmembrane conductance regulator, EMBO J. 23 (2004) 282–293.
[6] S.H. Cheng, R.J. Gregory, J. Marshall, S. Paul, D.W. Souza, G.A. White, C.R. Oriordan, A.E. Smith, Defective intracellular-transport and processing of cftr is the molecular-basis of most cystic-fibrosis, Cell 63 (1990) 827–834.
[7] W. Dalemans, P. Barbry, G. Champigny, S. Jallat, K. Dott, D. Dreyer, R.G. Crystal, A. Pavirani, J.P. Lecocq, M. Lazdunski, Altered chloride-ion channel kinetics associated with the delta-f508 cystic-fibrosis mutation, Nature 354 (1991) 526–528.
[8] E.A. Pasyk, J.K. Foskett, Mutant (delta-f508) cystic-fibrosis transmembrane conductance regulator cl-channel is functional when retained in endoplasmic-reticulum of mammalian-cells, J. Biol. Chem. 270 (1995) 12347–12350.
[9] C.L. Ward, R.R. Kopito, Intracellular turnover of cystic-fibrosis transmembrane conductance regulator-inefficient processing and rapid degradation of wild-type and mutant proteins, J. Biol. Chem. 269 (1994) 25710–25718.
[10] R.R. Kopito, Biosynthesis and degradation of cftr, Physiol. Rev. 79 (1999) S167–S173.
[11] R.R. Kopito, Aggresomes, inclusion bodies and protein aggregation, Trends Cell Biol. 10 (2000) 524–530.
[12] G.M. Denning, M.P. Anderson, J.F. Amara, J. Marshall, A.E. Smith, M.J. Welsh, Processing of mutant cystic-fibrosis transmembrane conductance regulator is temperature-sensitive, Nature 358 (1992) 761–764.
[13] R.L. Dormer, R. Derand, C.M. McNeilly, Y. Mettey, L. Bulteau-Pignoux, T. Metaye, J.M. Vierfond, M.A. Gray, L.J.V. Galietta, M.R. Morris, M.M.C. Pereira, I.J.M. Doull, F. Becq, M.A. McPherson, Correction of delf508-cftr activity with benzo(c)quinolizinium compounds through facilitation of its processing in cystic fibrosis airway cells, J. Cell Sci. 114 (2001) 4073–4081.
[14] O. Eidelman, M. Srivastava, J. Zhang, X. Leighton, J. Murtie, C. Jozwik, K. Jacobson, D.L. Weinstein, E.L. Metcalf, H.B. Pollard, Control of the proinflammatory state in cystic fibrosis lung epithelial cells by genes from the tnf-alpha r/nf kappa b pathway, Mol. Med. 7 (2001) 523–534.
[15] B.E. Cohen, G. Lee, K.A. Jacobson, Y.C. Kim, Z. Huang, E.J. Sorscher, H.B. Pollard, 8-cyclopentyl-1,3-dipropylxanthine and other xanthines differentially bind to the wild-type and delta f508 mutant first nucleotide binding fold (nbf-1) domains of the cystic fibrosis transmembrane conductance regulator, Biochemistry 36 (1997) 6455–6461.
[16] B.H. Qu, E.H. Strickland, P.J. Thomas, Localization and suppression of a kinetic defect in cystic fibrosis transmembrane conductance regulator folding, J. Biol. Chem. 272 (1997) 15739–15744.
[17] B.H. Qu, P.J. Thomas, Alteration of the cystic fibrosis transmembrane conductance regulator folding pathway—effects of the delta f508 mutation on the thermodynamic stability and folding yield of nbd1, J. Biol. Chem. 271 (1996) 7261–7264.
[18] M.A. Bianchet, Y.H. Ko, L.M. Amzel, P.L. Pedersen, Modeling of nucleotide binding domains of abc transporter proteins based on a f-1-atpase/reca topology: structural model of the nucleotide binding domains of the cystic fibrosis transmembrane conductance regulator (cftr), J. Bioenerg. Biomembr. 29 (1997) 503–524.
[19] X.Q. Zou, T.C. Hwang, Atp hydrolysis-coupled gating of cftr chloride channels: structure and function, Biochemistry 40 (2001) 5579–5586.
[20] I.D. Kerr, Structure and association of atp-binding cassette transporter nucleotide-binding domains, Biochim. Biophys. Acta-Biomembr. 1561 (2002) 47–64.
[21] Sybyl, version 6.7.1, Tripos Inc, 1699 South Hanley Rd, St Louis, Missouri, 63144, USA.
[22] H.A. Lewis, Z.X. Wang C., J.M. Sauder, I. Rooney, B.W. Noland, D. Lorimer, M.C. Kearins, K. Conners, B. Condon, P.C. Maloney, W.B. Guggino, J.F. Hunt, S. Emtage, Impact of the deltaf508 mutation in first nucleotide-binding domain of human cystic fibrosis transmembrane conductance regulator on domain folding and structure, J. Biol. Chem. 280 (2005) 1346–1353.
[23] B.H. Besler, K.M. Merz, P.A. Kollman, Atomic charges derived from semiempirical methods, J. Comput. Chem. 11 (1990) 431–439.
[24] U.C. Singh, P.A. Kollman, An approach to computing electrostatic charges for molecules, J. Comput. Chem. 5 (1984) 129–145.
[25] M.J. Frisch, G.W. T, H.B. Schlegel, G.E. Scuseria, M.A. Robb, J.R. Cheeseman, V.G. Zakrzewski, J.A. Montgomery Jr., R.E. Stratmann, J.C. Burant, S. Dapprich, J.M. Millam, A.D. Daniels, K.N. Kudin, M.C. Strain, O. Farkas, J. Tomasi, V. Barone, M. Cossi, R. Cammi, B. Mennucci, C. Pomelli, C. Adamo, S. Clifford, J. Ochterski, G.A. Petersson, P.Y. Ayala, Q. Cui, K. Morokuma, D.K. Malick, A.D. Rabuck, K. Raghavachari, J.B. Foresman, J. Cioslowski, J.V. Ortiz, A.G. Baboul, B.B. Stefanov, G. Liu, A. Liashenko, P. Piskorz, I. Komaromi, R. Gomperts, R.L. Martin, D.J. Fox, T. Keith, M.A. Al-Laham, C.Y. Peng, A. Nanayakkara, M. Challacombe, P.M.W. Gill, B. Johnson, W. Chen, M.W. Wong, J.L. Andres, C. Gonzalez, M. Head-Gordon, E.S. Replogle, J.A. Pople, Gaussian 98, 1998.
[26] J.M. Wang, R.M. Wolf, J.W. Caldwell, P.A. Kollman, D.A. Case, Development and testing of a general amber force field, J. Comput. Chem. 25 (2004) 1157–1174.
[27] D.A. Case, D.A. P, J.W. Caldwell, T.E. Cheatham III, J. Wang, W.S. Ross, C.L. Simmerling, T.A. Darden, K.M. Merz, R.V. Stanton, A.L. Cheng, J.J. Vincent, M. Crowley, V. Tsui, H. Gohlke, R.J. Radmer, Y. Duan, J. Pitera, I. Massova, G.L. Seibel, U.C. Singh, P.K. Weiner, P.A. Kollman, Amber 7, 2002.
[28] C.I. Bayly, P. Cieplak, W.D. Cornell, P.A. Kollman, A well-behaved electrostatic potential based method using charge restraints for deriving atomic charges—the resp model, J. Phys. Chem. 97 (1993) 10269–10280.
[29] W.D. Cornell, P. Cieplak, C.I. Bayly, I.R. Gould, K.M. Merz, D.M. Ferguson, D.C. Spellmeyer, T. Fox, J.W. Caldwell, P.A. Kollman, A 2nd generation force-field for the simulation of proteins, nucleic-acids, and organic-molecules, J. Am. Chem. Soc. 117 (1995) 5179–5197.
[30] W.L. Jorgensen, J. Chandrasekhar, J.D. Madura, R.W. Impey, M.L. Klein, Comparison of simple potential functions for simulating liquid water, J. Chem. Phys. 79 (1983) 926–935.
[31] J.P. Ryckaert, G. Ciccotti, H.J.C. Berendsen, Numerical-integration of cartesian equations of motion of a system with constraints—molecular-dynamics of *n*-alkanes, J. Comput. Phys. 23 (1977) 327–341.
[32] T. Darden, D. York, L. Pedersen, Particle mesh ewald—an *n*.Log(*n*) method for ewald sums in large systems, J. Chem. Phys. 98 (1993) 10089–10092.
[33] H.J.C. Berendsen, J.P.M. Postma, W.F. Vangunsteren, A. Dinola, J.R. Haak, Molecular-dynamics with coupling to an external bath, J. Chem. Phys. 81 (1984) 3684–3690.
[34] D.A. Case, T.A. D, T.E. Cheatham III, C.L. Simmerling, J. Wang, R.E. Duke, R. Luo, K.M. Merz, B. Wang, D.A. Pearlman, M. Crowley, S. Brozell, V. Tsui, H. Gohlke, J. Mongan, V. Hornak, G. Cui, P. Beroza, C. Schafmeister, J.W. Caldwell, W.S. Ross, P.A. Kollman, Amber 8, 2004.
[35] E.F. Pettersen, T.D. Goddard, C.C. Huang, G.S. Couch, D.M. Greenblatt, E.C. Meng, T.E. Ferrin, Ucsf chimera—a visualization system for exploratory research and analysis, J. Comput. Chem. 25 (2004) 1605–1612.
[36] C.F. Higgins, K.J. Linton, The atp switch model for abc transporters, Nat. Struct. Mol. Biol. 11 (2004) 918–926.
[37] Y.H. Ko, P.J. Thomas, M.R. Delannoy, P.L. Pedersen, The cystic-fibrosis transmembrane conductance regulator—overexpression, purification, and characterization of wild-type and delta-f508 mutant forms of the 1st nucleotide-binding fold in fusion with the maltose-binding protein, J. Biol. Chem. 268 (1993) 24330–24338.

[38] D.C.A. Neville, C.R. Rozanas, B.M. Tulk, R.R. Townsend, A.S. Verkman, Expression and characterization of the nbd1-r domain region of cftr: evidence for subunit–subunit interactions, Biochemistry 37 (1998) 2401–2409.

[39] A. Amadei, M.A. Ceruso, A. Di Nola, On the convergence of the conformational coordinates basis set obtained by the essential dynamics analysis of proteins' molecular dynamics simulations, Proteins-Struct. Funct. Genet. 36 (1999) 419–424.

[40] A. Amadei, A.B.M. Linssen, H.J.C. Berendsen, Essential dynamics of proteins, Proteins-Struct. Funct. Genet. 17 (1993) 412–425.

[41] A.E. Garcia, Large-amplitude nonlinear motions in proteins, Phys. Rev. Lett. 68 (1992) 2696–2699.

[42] M. Aschi, D. Roccatano, A. Di Nola, C. Gallina, E. Gavuzzo, G. Pochetti, M. Pieper, H. Tschesche, F. Mazza, Computational study of the catalytic domain of human neutrophil collagenase. Specific role of the s-3 and s'(3) subsites in the interaction with a phosphonate inhibitor, J. Comput. Aid. Mol. Des. 16 (2002) 213–225.

[43] A. Merlino, L. Vitagliano, M.A. Ceruso, L. Mazzarella, Subtle functional collective motions in pancreatic-like ribonucleases: from ribonuclease a to angiogenin, Proteins-Struct. Funct. Genet. 53 (2003) 101–110.

[44] P.H. Thibodeau, C.A. Brautigam, M. Machius, P.J. Thomas, Side chain and backbone contributions of phe508 to cftr folding, Nat. Struct. Mol. Biol. 12 (2005) 10–16.